Neutron Particle Hole Structure in ^{208}Pb†

C. FRED MOORE, J. G. KULLECK, AND PETER VON BRENTANO
The University of Texas, Austin, Texas

AND

FRANK RICKEY
Los Alamos Scientific Laboratory, University of California, Los Alamas, New Mexico

(Received 5 July 1967)

The ^{208}Pb(p,p') reaction was studied at twelve energies between 14 and 18 MeV, using a magnetic spectrograph placed at 90°. Excitation energies of states in ^{208}Pb have been measured up to 7-MeV. Spectra taken on analog resonances in ^{209}Bi exhibit many preferentially populated particle-hole states in ^{208}Pb. Qualitative information about the structure of these states is given.

INTRODUCTION

INFORMATION on excited states of doubly magic nuclei is of interest to nuclear structure theory. A particularly interesting case is the nucleus ^{208}Pb. The low-lying states in ^{207}Pb, ^{209}Pb, and ^{209}Bi are believed to be pure single-particle states. Because of the large energy gap between filled and unfilled shells, we expect many of the low-lying excited states of ^{208}Pb to be rather pure particle-hole excitations. The intent of this paper is to determine experimentally the positions and the dominant particle configurations of the neutron-hole states in ^{208}Pb. The method employed is analog resonant inelastic proton scattering on ^{208}Pb. If the resonances (in ^{209}Bi) are the isobaric analogs of pure single-particle neutron states in ^{209}Pb, then these resonances should decay preferentially to particle-hole states in ^{208}Pb. In a previous communication,[1] we have studied the (5^-, 3.192-MeV) and (4^-, 3.469-MeV) states in ^{208}Pb and have confirmed by means of resonant inelastic scattering that these states have the dominant configuration $g_{9/2}$ neutron, $p_{1/2}$ hole. The present work extends this study to many higher excited states in ^{208}Pb. These results are compared with previous work.[2–8]

EXPERIMENTAL METHOD

The proton beam was produced using the LASL 3-stage Van de Graaff accelerator. The target was a self-supporting ^{208}Pb (99.3% enriched) metallic foil of 0.7 mg/cm^2 thickness, mounted in transmission position at an angle of 45°. The scattered protons were measured at a laboratory angle of 90° using an Elbeck spectrograph. A total of twelve exposures were made at incident proton energies of 14.950, 15.020, 15.085, 16.450, 16.550, 16.650, 16.800, 16.900, 17.000, 17.100, 17.400, and 17.500 MeV. The spectrograph's field remained constant throughout the duration of these exposures. A self-consistent energy calibration was made, and the resulting excitation energies obtained for the various proton groups (including those from ^{12}C and ^{16}O) had a standard deviation of less than 3 keV throughout the twelve runs. This is within the experimental resolution of 9 keV full width at half maximum (FWHM). Since the level density in ^{208}Pb is quite high between 4 and 7 MeV, and since the cross sections change rapidly owing to the presence of the analog resonances, identification of levels is experimentally difficult. For this reason it was necessary to obtain high resolution and an accurate energy calibration.

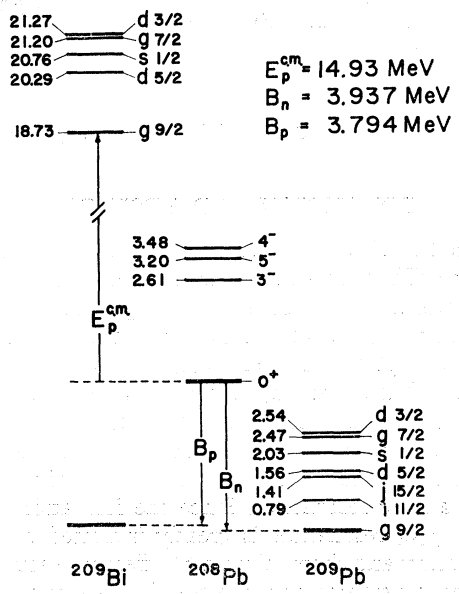

FIG. 1. Level diagrams showing the nuclear states of interest in ^{209}Pb, ^{208}Pb, and ^{209}Bi. Only the first four levels in ^{208}Pb are shown. Table I gives the complete listing of levels observed in ^{208}Pb. The levels in ^{209}Pb are taken from Ref. 8 and the analog levels in ^{209}Bi are taken from Refs. 9–11. For simplicity the neutron-proton mass difference has been disregarded.

† Supported in part by the U. S. Atomic Energy Commission.

[1] C. Fred Moore, L. J. Parish, P. von Brentano, and S. A. A. Zaidi, Phys. Letters **22**, 616 (1966); S. A. A. Zaidi *et al.* (to be published).

[2] Ole Hansen and O. Nathan (private communication).

[3] J. H. Bjerregaard, Ole Hansen, and O. Nathan, Nucl. Phys. **89**, 337 (1966).

[4] John Erskine (private communication).

[5] J. Bardwick and R. Tickle, Phys. Rev. **161**, 1217 (1967).

[6] R. K. Jolly, E. K. Lin, and B. L. Cohen, Phys. Rev. **128**, 2292 (1962).

[7] J. Sandinos, G. Vallois, O. Beer, M. Gendrot, and P. Lopato, Phys. Letters **22**, 492 (1966).

[8] P. Mukherjee and B. L. Cohen, Phys. Rev. **127**, 1284 (1962).

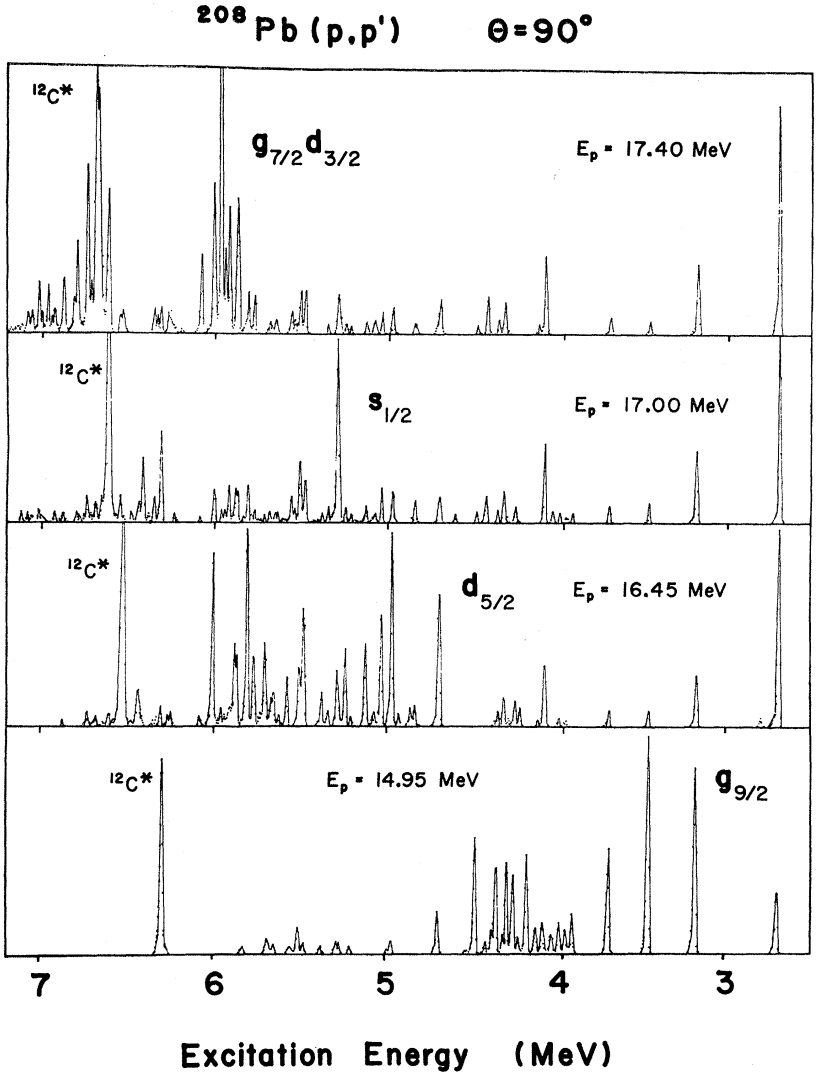

FIG. 2. Inelastic proton spectra taken at 90° near the $g_{9/2}$ analog resonance, $E_p=14.95$ MeV; the $d_{5/2}$ analog resonance, $E_p=16.45$ MeV; the $s_{1/2}$ analog resonance, $E_p=17.0$ MeV; and the $g_{7/2}-d_{3/2}$ analog resonance, $E_p=17.4$ MeV. The ground-state elastic proton group was deleted from this figure in order to expand the region of interest. Full scale is approximately 500 counts per $\frac{1}{4}$ mm track. In the case where there was a gap between plates, data points from exposures at adjacent energies were used.

DISCUSSION AND RESULTS

Figure 1 is a level diagram showing the single-particle states in ^{209}Pb, their analog states in ^{209}Bi, and the low-lying states in ^{208}Pb. Since the analog resonances have widths of the order of 250 keV, all of the resonances overlap except for the relatively isolated $g_{9/2}$ analog resonance. The $g_{7/2}$ and $d_{3/2}$ resonances are separated by only 50 keV. Additional spectra were taken around the resonance energies in order to determine when and if a particular final state is fed by one or more of the overlapping analog resonances. Since the formation of the $i_{11/2}$ and $j_{15/2}$ resonances is greatly inhibited by small penetrability and shows almost no effect in elastic scattering, we considered only the $g_{9/2}$, $d_{5/2}$, $s_{1/2}$, and the unresolved $g_{7/2}-d_{3/2}$ resonances. Spectra which were taken on these resonances are shown in Fig. 2, the resonance energies being known from previous work.[9-11] It is apparent that the cross section for the states in the spectrum up to 7 MeV in excitation resonante very strongly, a behavior similar to that found by Allan[12] for the reaction ^{118}Sn(p,p'). In particular, one can see that each resonance populates distinct groups of levels. Even though we will not be able to give a quantitative analysis of the experiment, the effects seen are so strong that a qualitative analysis will give us information about the strength of the particle-hole configuration contained in the various states in ^{208}Pb which are observed in the spectra.

In a qualitative way it is very easy to see which states are populated in the isospin-allowed proton decay of an isobaric analog state. The decay is determined purely by the doorway configuration of the analog resonance

[9] C. F. Moore, Bull. Am. Phys. Soc. **11**, 97 (1966).

[10] C. D. Kavaloski, J. S. Lilley, P. Richard, and N. Stein, Phys. Rev. Letters **16**, 807 (1966).

[11] G. H. Lenz and G. M. Temmer, Phys. Letters (to be published).

[12] D. L. Allan, Phys. Letters **14**, 311 (1965).

ψ_A, and this doorway configuration of the analog state ψ_A is:

$$\psi_A=\frac{1}{(2T+1)^{1/2}}\mathbf{T}^-\psi_{PA}=\frac{1}{(2T+1)^{1/2}}(\sum_i \mathbf{t}_i^-)\psi_{PA}.$$

In this relation $T+\frac{1}{2}$ is the isospin of the parent analog state, and $\mathbf{t}_i^-$ is the isospin-lowering operator acting on the particle "i". For the case of a parent analog with a single-neutron configuration, $\psi_{PA}=\phi_n\psi_{cs}$, where ψ_{cs} is the wave function for the closed-shell core of the ground state of ^{208}Pb, and ϕ_n is the wave function for a neutron in the shell-model state "J". We have represented the wave function ψ_A in a schematic way in Fig. 3 for the analog of the ground state of ^{209}Pb.

The first term in this expression represents a single-proton configuration. This explains why the analog states in ^{209}Bi can easily be formed by elastic proton scattering on the core, ^{208}Pb. The other terms are two-particle–one-hole configurations (one proton, one neutron, and one hole where the proton and hole occupy the same shell-model state). The protons in these configurations are unbound, and they can penetrate the Coulomb barrier and leave the nucleus. The residual states populated from the decay of the analog of the single-neutron state are then the neutron-hole states. It is obvious that the same state could, in principle, be populated in a neutron pickup reaction performed on the parent analogue state ψ_{PA}. From the measurement of a strong proton decay of the analog resonance of spin J, we can immediately infer that the final state has a dominant particle-hole configuration of the form $(J,j^{-1})_I\psi_{cs}$, in which a particle of angular momentum J is coupled to a hole of angular momentum j to give a state of spin I. If we know J, we do not know necessarily the spin j of the hole, except that it is most likely

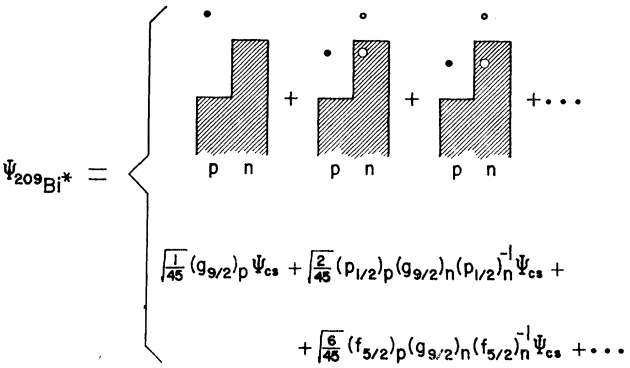

FIG. 3. Schematic diagram showing the particle representation of the analog of the ground state of ^{209}Pb. The figure shows only the first three terms for the configuration of the wave function of the $g_{9/2}$ analog state in ^{209}Bi. The remaining terms are (proton, neutron, hole) configurations of $3p_{3/2}$, $1i_{13/2}$, $2f_{7/2}$, and $1h_{9/2}$, coupled to the $g_{9/2}$ neutron. These remaining terms are two-particle–one-hole configurations similar to the second and third term as shown. The shell-model states between $n=82$ and 126 can be seen in Fig. 4. The wave functions shown must still be antisymmetrized. The proton and neutron hole are coupled to be zero.

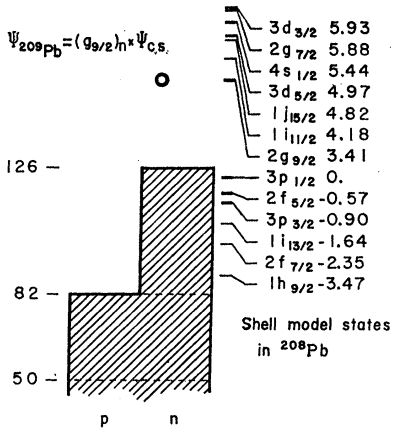

FIG. 4. Configuration diagram of the ground state of ^{209}Pb together with a listing of shell model states. The particle states are listed as observed in ^{208}Pb$(d,p)^{209}$Pb, while the hole states are taken from the ^{208}Pb$(d,t)^{207}$Pb spectra (Ref. 8).

$p_{1/2}$, $f_{5/2}$, or $p_{3/2}$. These hole configurations are the ones closest to the Fermi surface as shown in Fig. 4. We have omitted the $i_{13/2}$ and $h_{9/2}$ hole states because they will be populated only very weakly owing to the low barrier penetration of particles with high angular momentum ($l=5$ and $l=6$).

In order to illustrate this argument, consider the second term of the expression in Fig. 3:

$$(g_{9/2})_n\{(p_{1/2})_n^{-1}(p_{1/2})_p\}_{I=0}\psi_{cs}.$$

It is quite obvious that we can recouple the angular momentum involved in the expression so that it becomes a proton coupled to the neutron-hole state:

$$(p_{1/2})_p\{(g_{9/2})_n(p_{1/2})_n^{-1}\}_{I=4}\psi_{cs}$$
$$\text{or } (p_{1/2})_p\{(g_{9/2})_n(p_{1/2})_n^{-1}\}_{I=5}\psi_{cs}.$$

This is in agreement with the observed decay of the

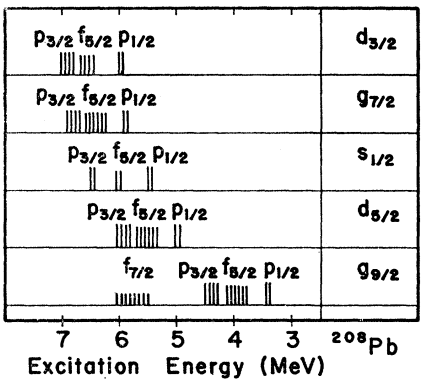

FIG. 5. Schematic picture giving the centroid energy of the unperturbed neutron hole states in ^{208}Pb. Also shown is the number of states with different spins which can be formed from the configurations. The spread of the group about the centroid energy is for graphical purposes only and without significance. The centroid energies are calculated from the experimental energies of the single particle and hole states in ^{209}Pb and ^{207}Pb as given by Mukerjee and Cohen (Ref. 8), shown in Fig. 4.

TABLE I. Experimental results. Absolute cross sections are determined to within 25%, whereas the relative cross sections are determined

^{209}Bi(t,α)[a]			^{206}Pb(t,p)[b]			^{207}Pb(d,p)[c]		^{207}Pb(d,p)[d]			^{208}Pb(d,d')[e]		^{208}Pb(p,p')[f]		
E_x (MeV)	S	J^π	E_x (MeV)	$\Sigma \frac{d\sigma}{d\Omega}$	J^π	E_x (MeV)	172° yield	E_x (MeV)	$\Sigma \frac{d\sigma}{d\Omega}$	$\lvert n\rangle$	E_x (MeV)	60° yield	E_x (MeV)	β_l	J^π
2.60	0.1	3^-	2.62	21	3^-	2.619	(0.01)	2.62	0.049		2.61	240	2.614	0.085	3^-
3.20	0.06	5^-	3.20	45	5^-	3.199	0.15	3.19	2.2	$2g_{9/2}$	3.20	44	3.198	0.051	5^-
3.48	(0.003)	4^-				3.475	0.10	3.47	2.0	$2g_{9/2}$	3.48	11	3.476	0.011	4^-
3.71	0.3	5^-				3.706	0.026	3.73 3.76	0.35	$2g_{9/2}$	3.71	9	3.709	0.024	5^-
													3.910		
3.96	1.0	$(4^-, 5^-)$											3.950		
											3.97	8			
													3.990		
			4.04	5									4.025	(0.020)	(4^-)
											4.08	11	4.070	0.041	2^+
													4.155		
													4.185		
													4.215		
								4.22 4.28	0.39	$1i_{11/2}$ $2g_{9/2}$			4.240		
											4.33	20	4.305	0.047	4^+
													4.405	0.040	6^+
											4.47	8	4.465		
			4.62	5				4.61	0.13	$1j_{15/2}$	4.59	6	4.600	0.032	8^+
			4.71	17		4.707	0.25	4.70	1.1	$3d_{5/2}$			4.690		(10^+)
								4.83 4.86	0.25	$1j_{15/2}$	4.83	9	4.840		
			4.87	45	0^+								4.867		
													4.917		
			4.98	42		4.979	0.43	4.98	2.0	$3d_{5/2}$			4.968		
						5.039	0.78	5.03	1.9	$3d_{5/2}$			5.036		
													5.084		
						5.132	0.29	5.12	1.0	$3d_{5/2}$			5.126		
													5.220		
			5.25	15		5.250	0.36	5.24	1.1	$3d_{5/2}$			5.246		
			5.30	47		5.294	1.87	5.28	2.2	$4s_{1/2}$			5.285		
													5.357		
						5.392	(0.06)						5.386		
													5.424		
			5.49	7									5.478		
			5.52	36		5.518	(0.09)						5.508		
			5.56	72		5.559	(0.08)						5.550		
						5.604	0.08								
			5.65	22									5.650		
			5.70	7									5.687		
						5.789	0.114	5.77 5.80	0.46	$3d_{3/2}$					
			5.82	40									5.82		
								5.85	1.2	$2g_{7/2}$					
			5.88	7		5.882	0.160	5.89	1.5	$3d_{3/2}$					
			5.93	69		5.933	0.75	5.93	1.2	$3d_{3/2}$					
			5.96	24		5.952	0.54	5.96	2.5	$2g_{7/2}$					
			5.99	19				6.00	0.66	$2g_{7/2}$					
			6.04					6.05	0.62	$3d_{3/2}$					
			6.07					6.07							
			6.11	15		6.096	0.27								

[a] Hansen and Nathan, Ref. 2.
[b] Bjerregaard, Hansen, and Nathan, Ref. 3.
[c] Erskine, Ref. 4.
[d] Bardwick and Tickle, Ref. 5.
[e] Jolly, Lin, and Cohen, Ref. 6.
[f] Sandinos, Vallois, Beer, Gendrot, and Lopato, Ref. 7.
[g] Gap between plates.
[h] Obscured by the first excited state of ^{12}C.

to within counting statistics. Number of counts ≈4.2× (number of μb). ···indicates too few counts to determine cross section.

	Cross section (microbarns per steradian) for incident proton energies as listed														
E_x (MeV)	14.950	15.020	15.085	16.450	16.550	16.650	16.800	16.900	17.000	17.100	17.400	17.500	$\|n\rangle$	$\|n\rangle^{-1}$	J^π
2.608	147.1	201.1	211.0	353.8	350.4	351.8	353.3	333.4	gap[g]	378.5	(412.8)	(511.4)		collective	
3.192	365.3	357.1	254.9	103.2	106.3	124.8	138.0	133.9	125.0	133.9	127.2	127.9	$g_{9/2}$	$p_{1/2}$	5^-
3.469	426.2	371.0	237.4	28.1	35.5	26.2	29.0	25.0	25.4	25.7	22.6	···	$g_{9/2}$	$p_{1/2}$	4^-
3.702	189.1	167.5	117.4	30.0	35.0	(20.9)	33.6	32.4	30.2	36.5	28.8	(19.7)	$g_{9/2}$		
3.913	(50.4)	115.2	78.5	···	···	···	···	···	(13.2)	···	···	(8.6)	$g_{9/2}$		
3.955	gap	64.3	46.8	(10.1)	17.3	(12.7)	17.3	···	(8.9)	(17.8)	···	···	$g_{9/2}$		
3.992	gap	21.6	52.3	(9.6)	(15.8)	(14.4)	(13.4)	10.8	(15.4)	(14.6)	···	···			
4.032	gap	gap	46.3	···	(11.5)	(11.3)	(14.4)	(18.0)	(21.4)	31.2	···	···			
4.080	60.7	gap	gap	121.9	123.4	124.1	129.6	143.0	128.6	140.9	139.9	135.4		collective	
4.117	53.5	gap	(8.9)	(5.0)	···	···	···	···	···	21.8	···	···	$g_{9/2}$		
4.174	177.1	113.3	···	···	···	···	···	···	···	···	···	···	$g_{9/2}$	$f_{5/2}$, $p_{3/2}$	
4.225	32.9	22.6	20.6	36.0	33.4	(10.3)	···	···	···	(6.7)	···	···	$g_{9/2}$		
4.252	173.8	121.2	90.0	50.6	55.0	52.8	39.1	33.4	35.0	39.1	···	34.6	$g_{9/2}$	$f_{5/2}$, $p_{3/2}$	
4.289	186.2	118.1	97.9	(11.8)	21.1	···	···	19.0	···	(13.9)	···	···	$g_{9/2}$	$f_{5/2}$, $p_{3/2}$	
4.317	···	39.8	40.1	46.3	44.4	49.2	44.4	58.3	52.8	57.1	57.6	58.8		collective	
4.351	184.1	137.0	111.8	28.6	29.8	36.7	···	···	(17.8)	(5.0)	(23.8)	···	$g_{9/2}$	$f_{5/2}$, $p_{3/2}$	
4.419	17.5	···	···	···	···	52.3	45.4	52.1	53.5	50.2	75.1	61.0			
4.475	225.4	152.2	104.6	···	···	···	23.8	(8.2)	18.5	(11.0)	(8.6)	···	$g_{9/2}$		
4.602	···	···	···	···	···	11.8	···	···	(5.5)	(14.6)	···	···			
4.692	93.6	64.1	58.6	268.6	234.2	123.1	75.4	56.2	63.4	66.0	75.8	69.6	$d_{5/2}$	$p_{1/2}$	3^-
4.835	···	···	32.4	37.9	43.4	49.0	42.2	41.8	46.8	46.6	(10.8)	51.8		collective	
4.857	···	···	···	27.6	(25.2)	···	···	···	···	···	···	···	$d_{5/2}$		
4.928	···	···	···	20.6	···	(16.6)	···	···	···	(22.3)	···	30.7			
4.967	29.0	25.9	26.2	331.7	293.0	153.8	78.7	52.1	60.0	54.5	56.2	38.4	$d_{5/2}$	$p_{1/2}$	2^-
5.030	···	···	···	225.1	237.1	147.4	91.7	50.6	45.4	42.2	34.8	···	$d_{5/2}$		
5.071	···	···	···	31.2	29.0	24.7	···	···	···	25.7	35.0	42.5			
5.121	···	···	13.4	150.0	135.8	80.2	35.3	(21.8)	28.6	20.4	(16.8)	(11.0)	$d_{5/2}$		
5.205	15.1	...	···	19.2	33.1	16.1	···	···	(16.8)	···	(10.8)	···			
5.238	···	(7.9)	···	145.7	136.3	78.2	35.0	(22.1)	26.2	21.4	23.0	(18.5)	$d_{5/2}$		
5.284	26.6	25.7	24.0	107.8	127.2	142.6	201.1	301.7	356.6	232.8	85.9	66.7	$s_{1/2}$	$p_{1/2}$	1^-
5.338	···	···	···	31.0	(29.8)	(26.6)	25.7	(22.8)	26.9	23.5	14.9	31.2		collective	
5.373	(9.4)	14.6	···	67.0	···	49.4	26.9	24.7	(10.6)	23.0	···	···			
5.474	25.0	19.2	···	gap	301.0	211.7	130.3	111.4	106.1	101.3	98.9	91.4	$d_{5/2}$		
5.505	55.0	41.8	56.4	gap	(107.8)	139.7	119.0	133.2	120.0	113.0	79.9	81.6	$s_{1/2}$	$p_{1/2}$	0^-
5.536	···	···	···	gap	gap	···	···	28.8	···	···	(23.3)	40.8			
5.554	18.7	···	(11.5)	82.3	gap	77.8	51.1	55.2	(49.0)	55.7	49.0	(55.7)			
5.646	23.0	21.4	···	24.7	gap	gap	35.5	28.8	···	37.7	31.7	(13.4)			
5.679	42.5	29.8	19.7	90.5	gap	gap	···	···	(20.9)	···	25.7	···			
5.703	···	···	(12.5)	166.3	45.4	gap	gap	···	(8.6)	···	···	···	$d_{5/2}$		
5.769	···	···	···	153.4	81.6	62.9	gap	32.9	24.7	35.8	62.7	59.8	$d_{5/2}$		
5.804	···	···	···	389.3	211.9	191.5	gap	84.2	67.0	88.8	95.5	103.9	$d_{5/2}$, $d_{3/2}$	$p_{1/2}$, $p_{3/2}$	
5.869	···	···	···	215.8	126.2	121.4	gap	gap	98.4	95.8	282.5	261.6	$d_{5/2}$, $d_{3/2}$	$p_{1/2}$, $p_{3/2}$	
5.914	···	···	···	···	···	36.7	(29.0)	gap	69.6	77.0	219.7	241.0	$g_{7/2}$	$p_{1/2}$	
5.936	···	···	···	···	···	(23.0)	···	gap	gap	···	(161.8)	(159.8)	$d_{3/2}$	$p_{1/2}$	
5.958	···	···	···	32.2	···	31.7	36.2	gap	gap	91.9	577.4	445.0	$g_{7/2}$	$p_{1/2}$	
6.000	···	···	···	341.3	189.1	155.8	···	56.4	gap	102.0	268.1	235.0	$d_{5/2}$, $d_{3/2}$	$p_{1/2}$, $p_{3/2}$	
6.078	···	···	···	21.4	···	21.8	19.7	···	gap	gap	121.9	117.6	$d_{3/2}$	$p_{1/2}$	

TABLE I.

^{209}Bi(t,α)[a]			^{206}Pb(t,p)[b]			^{207}Pb(d,p)[c]		^{207}Pb(d,p)[d]			^{208}Pb(d,d')[e]		^{208}Pb(p,p')[f]		
E_x (MeV)	S	J^π	E_x (MeV)	$\Sigma \frac{d\sigma}{d\Omega}$	J^π	E_x (MeV)	172° yield	E_x (MeV)	$\Sigma \frac{d\sigma}{d\Omega}$	$\lvert n\rangle$	E_x (MeV)	60° yield	E_x (MeV)	β_1	J^π
			6.20												
			6.47												
			6.52												
			6.57												
			6.61												
			6.70												
			6.76	23											
			6.79												
			6.83												
			6.88												
			6.90												
			6.93												
			6.97												
			7.00												
			7.03												
			7.07												
			7.10												

$g_{9/2}$ analog resonance to the (4^-, 3.485-MeV) and (5^-, 3.198 MeV) states in ^{208}Pb.

In Fig. 5 we have plotted the centroid energies of the unperturbed neutron-hole states in ^{208}Pb and the number of states with different spin which can be made from a particle-hole configuration. From a comparison of Fig. 5 and the data in Fig. 2, we see a remarkable similarity which indicates that the particle-hole states in ^{208}Pb are relatively pure. Also, particle-hole states with different particle angular momentum J seem to mix only very weakly.

Up to now we have discussed the ideal situation; the real situation is somewhat more complicated and we want to discuss briefly some of these features. The observed cross section is not entirely due to analog resonant scattering. There is a small contribution due to direct inelastic scattering. It has been demonstrated,[1] however, that the unnatural-parity states have a negligible direct cross section and that even for the natural-parity states the direct cross section is so weak that we can still obtain a reliable estimate of the resonant cross section from the peak cross section corrected for the background. For example, by comparing the excitation functions to the (5^-, 3.198-MeV) and (4^-,3.486-MeV) states, it can be seen that the former has a much higher off-resonance cross section. This is due to the fact that the 4^- state is an unnatural-parity state and can therefore be only excited in a direct reaction by spin flip. This observation may be used in some cases to provide a tentative method to decide whether a state has natural or unnatural parity. If we see a particular state at various resonances, this does not necessarily prove that it has a mixed configuration (noted as "collective" in Table I). We first have to show that the cross section indeed is enhanced at several resonances and that it does not simply arise from a direct process. This can be done quite easily by looking at the cross section at the additional energy points in Table I in the vicinity of the resonances.

Finally, we have discussed up to now only contributions to the resonant cross section coming from the doorway configuration. If the analog state is mixed, one expects a contribution to the cross section due to nearby compound states which have a lower isospin, which we might call compound inelastic scattering.[10] For example, it has been found that the excitation function to the (4^-, 3.486-MeV) state shows only the $g_{9/2}$ resonance.[1] Since we expect such compound inelastic scattering to be independent of any selection rules in the exit channel and consequently resonate at each analog state in each channel, we can therefore conclude that these contributions are small, and less than about 5% of the cross section to the 4^- state.

(*continued*).

E_x (MeV)	Cross section (microbarns per steradian) for incident proton energies as listed														
	14.950	15.020	15.085	16.450	16.550	16.650	16.800	16.900	17.000	17.100	17.400	17.500	|n⟩	$\|n\rangle^{-1}$	J^π
6.232	···	···	···	···	···	···	···	···	(11.5)	gap	···	···			
6.255	···	···	···	···	(23.3)	28.6	(7.7)	20.5	···	25.4	55.2	58.1			
6.304	h	···	···	35.3	42.5	59.5	114.0	166.3	161.8	104.2	45.1	30.5	$s_{1/2}$		
6.345	h	h	h	···	(9.1)	22.8	29.5	49.7	54.2	···	48.2	63.6			
6.377	···	···	···	···	···	···	···	···	(16.1)	···	gap	354.7	$d_{3/2}-g_{7/2}$		
6.409	···	···	···	···	31.4	52.8	78.2	110.4	120.5	79.9	gap	84.5	$s_{1/2}$		
6.436	···	···	···	91.2	158.6	···	(25.9)	31.4	···	57.4	gap	190.6	$d_{3/2}-g_{7/2}$		
6.480	···	···	···	···	···	···	···	···	(19.4)	···	gap	gap			
6.523	···	···	···	h	h	···	···	(4.6)	···	···	56.6	gap			
6.540	···	···	···	h	h	h	47.3	57.8	57.6	29.3	···	gap	$s_{1/2}$		
6.605	···	···	···	29.0	(12.2)	···	h	h	h	···	322.3	288.0	$d_{3/2}-g_{7/2}$		
6.646	···	···	···	···	···	···	···	48.7	···	h	h	145.2			
6.681	···	···	···	23.8	(17.8)	28.3	(25.0)	39.8	47.8	76.6	h	h			
6.730	···	···	···	28.3	(16.3)	31.0	35.3	41.8	53.0	62.9	320.4	302.2	$d_{3/2}-g_{7/2}$		
6.789	···	···	···	···	···	20.4	···	···	(15.6)	···	183.1	(128.6)	$d_{3/2}-g_{7/2}$		
6.807	···	···	···	···	···	···	···	···	(18.7)	36.2	(61.7)	82.6			
6.865	···	···	···	(6.5)	···	···	···	(12.2)	23.0	28.8	119.8	92.2			
6.917	···	···	···	···	···	19.2	(18.2)	21.4	21.1	28.3	50.4	69.6			
6.958	···	···	···	···	···	···	(14.9)	···	···	···	80.2	65.0			
6.989	···	···	···	···	···	···	···	···	···	(16.6)	(32.4)	(30.7)			
7.007	···	···	···	···	16.6	···	(11.0)	29.3	30.2	37.7	91.4	79.9			
7.051	···	···	···	···	19.0	19.2	19.9	22.6	(14.4)	(19.0)	50.6	45.1			
7.072	···	···	···	···	···	···	···	···	(12.2)	···	48.2	48.7			
7.108	···	···	···	···	(9.6)	(15.6)	···	···	20.1	(15.6)	(10.6)	...			

The determination of the angular momentum of the hole j in the dominant configuration of the particle-hole state is much more difficult. So also is the determination of the spin I of the final state. The best method of gaining this information is to measure angular distributions at the resonance energy. However, one may make a tentative estimate of j by comparing the centroid energy of one group of levels with another group of levels. This method can give some indication of j, especially since we expect the penetration factors for the emission of $f_{5/2}$ and $p_{3/2}$ protons to be very different. On the basis of these arguments we might think that the six states around 4 MeV excitation energy which are populated in the $g_{9/2}$ resonance have the dominant configuration $(g_{9/2})(f_{5/2})^{-1}$ and the four states at around 4.3 MeV excitation energy have the dominant configuration $(g_{9/2})(p_{3/2})^{-1}$. Similarly, we would assign the dominant configuration $(g_{9/2})(f_{7/2})^{-1}$ to a group of states seen in the $g_{9/2}$ resonance at an excitation energy between 5 and 6 MeV. Unfortunately, however, some of these states are either unresolved or collective, as indicated in Table I. Also, when a careful count is made of the states, there are too many. Consequently, we feel there is some truth in these naive assignments, but, in fact, the states are somewhat more complicated. Another method is to compare ^{208}Pb(p,p') with ^{207}Pb(d,p). In this experiment we know that the strong states seen will have a dominant configuration $(J, (p_{1/2})^{-1})_I$ and if we see a state strongly excited in both reactions we can thus determine the configuration for the hole j.

In Table I we have also given tentative assignments for the spins of states with the configurations $(d_{5/2})_n$ $(p_{1/2})_n^{-1}$ and $(s_{1/2})_n(p_{1/2})_n^{-1}$. These assignments are based mainly on the theoretical expectation that the higher spin state should have the lower energy as is the case for the 4^- and 5^- states from the $(g_{9/2})_n(p_{1/2})_n^{-1}$ configuration. An additional support for the assignment of the 1^- and 0^- spins is $(2I+1)$ in the reduced width which favors the 1^- state to have a bigger cross section. Also, these states are alternately of natural or unnatural parity. Consequently, their off-resonance cross section is used as an aid to determine their spin. This technique, however, is reduced in value since, despite the good resolution, there are too many unresolved states. The cross sections in Table I are deduced from the spectra using a consistent method which lacks the facility of distinguishing nearly unresolved states.

Assignments have been made in Table I based on the preceding discussion. We must emphasize, as is evident from our discussion, that the assignments of a hole angular momentum j and total spin I are at best only tentative. Also, the assignments of the particle angular momentum J for the states above 5.8 MeV in excitation

are tentative since there is evidence that the states are mixed and also since the $g_{7/2}$ and $d_{3/2}$ analog resonances are unresolved.

CONCLUSION

The interpretation of the data presented in this paper has been made as simple as possible. The data so far obtained are insufficient to satisfy the needs for a quantitative analysis since more complete excitation curves are required as well as angular distributions on the analog resonances. Our analysis makes rash assumptions concerning the purity of configurations of states. We think, however, that we have demonstrated that the quality of data obtained from resonant inelastic proton scattering on ^{208}Pb via analog states is indeed comparable to the quality of the data which we would expect from the equivalent neutron-pickup experiment on ^{209}Pb targets in various excited states, if this experiment were feasible. Another rather remarkable fact which can be seen from this experiment is that many particle-hole states in ^{208}Pb with excitation energies up to 6 MeV seem to be rather pure. We think this provides a good argument for the validity of a shell-model description for ^{208}Pb.

ACKNOWLEDGMENTS

We wish to thank Dick Woods for his help in obtaining the data at Los Alamos. Also, we thank Mrs. J. Page, Mrs. E. Jagger, and Mrs. C. Lee for their careful work in scanning the nuclear emulsion plates. Finally, we acknowledge the many illuminating discussions with S. Amir A. Zaidi and his helpful suggestions.

Errata

Fast-Neutron Scattering from Nuclides in the Lead Region, LAWRENCE CRANBERG, THOMAS A. OLIPHANT, JULES LEVIN, AND C. D. ZAFIROTOS [Phys. Rev. **159**, 969 (1967)]. A factor $(h/2m_\pi c)^2$ was inadvertently omitted from the spin-orbit term in the expressions for the optical potential. The spin-orbit potential strengths as given are numerically correct if we take them to be in units of MeV and include the above-mentioned factor in the expressions for the optical potential.

Coupled-Channel Schrödinger Equation Model for Neutron-Alpha and Deuteron-Triton Scattering. I, B. DE FACIO, R. K. UMERJEE, AND J. L. GAMMEL [Phys. Rev. **151**, 819 (1966)].

1. The ordinate on Fig. 4 should read "barns" instead of "mb."

2. The following transition matrix elements in Table V are misprinted:

$$\mathrm{Re}(t_{1,1}{}^{3/2}) = 0.10309 \quad \text{at} \quad 6 \text{ MeV},$$
$$\mathrm{Re}(t_{1,1}{}^{3/2}) = 0.10361 \quad \text{at} \quad 10 \text{ MeV},$$
$$\mathrm{Re}(t_{2,2}{}^{5/2}) = 0.1876 \quad \text{at} \quad 6 \text{ MeV},$$
$$\mathrm{Re}(t_{2,2}{}^{5/2}) = 0.1819 \quad \text{at} \quad 10 \text{ MeV}.$$

3. The calculated curve in Fig. 7 is wrong at 6 and 10 MeV in that it shows a forward peaking which does not follow from the reduced T-matrix elements of Table V and the potential of Table II. The corrected curve is flat from $\theta_{\mathrm{c.m.}} = 0$ to 100° and peaks at 180°. We thank Dr. J. E. Simmons and Dr. J. J. Malanify for pointing this out.

Orthogonal Classification of Alpha-Particle Wave Functions, JOHN E. BEAM* [Phys. Rev. **158**, 907 (1967)]. Equation (2) should be replaced by

$$\frac{\partial^2}{\partial \mathbf{r}_1{}^2}+\frac{\partial^2}{\partial \mathbf{r}_2{}^2}+\frac{\partial^2}{\partial \mathbf{r}_3{}^2}+\frac{\partial^2}{\partial \mathbf{r}_4{}^2}=\frac{\partial^2}{\partial \boldsymbol{\xi}_0{}^2}+\frac{\partial^2}{\partial \boldsymbol{\xi}_1{}^2}+\frac{\partial^2}{\partial \boldsymbol{\xi}_2{}^2}+\frac{\partial^2}{\partial \boldsymbol{\xi}_3{}^2},$$

and the sentence beginning in the ninth line after Table III should read,

"The number of S-independent scalars belonging . . . ."

* Present address: T. W. Bonner Nuclear Laboratories, Rice University, Houston, Texas.